This is the accepted manuscript made available via CHORUS. The article has been published as:

Constraining spectroscopic factors near the r-process path using combined measurements: ^{86}Kr (d, p)^{87}Kr

D. Walter, S. D. Pain, J. A. Cizewski, F. M. Nunes, S. Ahn, T. Baugher, D. W. Bardayan, T. Baumann, D. Bazin, S. Burcher, K. A. Chipps, G. Cerizza, K. L. Jones, R. L. Kozub, S. J. Lonsdale, B. Manning, F. Montes, P. D. O'Malley, S. Ota, J. Pereira, A. Ratkiewicz, P. Thompson, C. Thornsberry, and S. Williams

Phys. Rev. C **99**, 054625 — Published 24 May 2019

DOI: 10.1103/PhysRevC.99.054625

Constraining spectroscopic factors near the r-process path using combined measurements: ^{86}Kr(d,p)^{87}Kr

D. Walter,[1] S.D. Pain,[2] J.A. Cizewski,[1] F.M. Nunes,[3,4] S. Ahn,[3] T. Baugher,[1] D.W. Bardayan,[5] T. Baumann,[4] D. Bazin,[4] S. Burcher,[1] K.A. Chipps,[2,6] G. Cerizza,[6] K.L. Jones,[6] R.L. Kozub,[7] S.J. Lonsdale,[1,8] B. Manning,[1] F. Montes,[4,9] P.D. O'Malley,[5] S. Ota,[10] J. Pereira,[4] A. Ratkiewicz,[1] P. Thompson,[6,2] C. Thornsberry,[6] and S. Williams[4]

[1] *Department of Physics and Astronomy, Rutgers University, New Brunswick, NJ 08901 USA*
[2] *Physics Division, Oak Ridge National Laboratory, Oak Ridge, TN 37831 USA*
[3] *Department of Physics and Astronomy, Michigan State University, East Lansing, MI 48824 USA*
[4] *National Superconducting Cyclotron Laboratory, East Lansing, MI 48824 USA*
[5] *Department of Physics, University of Notre Dame, Notre Dame , IN 46556 USA*
[6] *Department of Physics, University of Tennessee, Knoxville, TN 37996*
[7] *Department of Physics, Tennessee Technological University, Cookeville, TN 38505*
[8] *Department of Physics, University of Surrey, Guildford GU2 7XH UK*
[9] *Joint Institute for Nuclear Astrophysics, Michigan State University, East Lansing, Michigan 48824, USA*
[10] *Japan Atomic Energy Agency, Tokai, Ibaraki, 319-1195, Japan*

(Dated: May 3, 2019)

Background: Modern nuclear structure models suggest that the shell structure near the valley of stability, with well-established shell closures at N=50, for example, changes in very neutron-rich nuclei far from stability. Single-particle properties of nuclei away from stability can be probed in single-neutron (d,p) transfer reactions with beams of rare isotopes. The interpretation of these data requires reaction theories with various effective interactions. Often, approximations made to the final bound-state potential introduce a large uncertainty in the extracted single-particle properties, in particular the spectroscopic factor.

Purpose: Mitigate this uncertainty using a combined measurement method to constrain the shape of the bound-state potential and to reliably extract the spectroscopic factor.

Methods: The ^{2}H(^{86}Kr,p)^{87}Kr reaction was measured at 33 MeV/u at the National Superconducting Cyclotron Laboratory (NSCL) as a test of the combined method. The reaction protons were detected with the Oak Ridge Rutgers University Barrel Array (ORRUBA) of position sensitive silicon strip detectors, the first implementation of ORRUBA coupled to the S800 spectrograph with fast beams at NSCL.

Results: These measurements at 33 MeV/u are combined with previous studies of the ^{86}Kr(d,p) reaction at 5.5 MeV/u to demonstrate a successful case of the combined method to constrain the shape of the single-particle potential and deduce asymptotic normalization coefficients and spectroscopic factors. In particular, the single-particle asymptotic normalization coefficient for the ground state of ^{87}Kr was constrained to $b_{d5/2}$=6.46 $^{+1.12}_{-0.57}$ fm$^{-1/2}$, and therefore the deduced spectroscopic factor is S=0.44 $^{+0.09}_{-0.13}$ with uncertainties dominated by experimental statistics.

Conclusions: By combining measurements at two very different beam energies, single-particle asymptotic normalization coefficients, at least for low angular momentum transfers, can be constrained. Therefore, spectroscopic factors can be deduced with uncertainties dominated by experimental uncertainties, rather than limited knowledge of bound-state potential parameters.

I. INTRODUCTION

The rapid neutron capture process (r-process) is the mechanism responsible for the creation of about half of the elements heavier than iron. This process is theorized to occur in stellar explosions or neutron star mergers where there is a very high neutron density (>10^{20} neutrons/cm^3) and high temperatures (>10^9 K). Recent r-process network calculations [1, 2] have highlighted the need to obtain better measurements of nuclear properties such as masses and neutron capture rates to understand the observed r-process abundances and to constrain the site of these events. This is especially important in the A∼80 region where more than one astrophysical phenomenon could contribute to the final observed abundances. Such studies have recognized that neutron capture at late times in an r-process event, when the neutron densities and/or temperatures are below the optimal values, can significantly affect the final abundances. Nuclei near the peaks in r-process abundances have closed shells of neutrons where the level densities are low and neutron capture is dominated by direct processes. Direct neutron capture is sensitive to the detailed spectroscopic properties of bound, low-spin states. Therefore, it is important to accurately measure the properties of neutron-rich nuclei near closed shells and near the r-process waiting points.

Single-nucleon transfer reactions such as (d,p), (p,d) or (d,n) are sensitive probes of the single-particle struc-

ture of exotic nuclei [3, 4]. To extract spectroscopic information on unstable nuclei, such reactions can be performed in inverse kinematics with beams of radioactive isotopes and light mass targets. The extracted spectroscopic properties can be used to constrain nuclear structure models, and therefore improve their reliability when predicting properties of nuclei further from stability. In addition, the measured spectroscopic factors are important in calculating the direct-semidirect component of neutron capture needed to understand observed r-process abundances (*e.g.* [5, 6]). The present work focuses on the neutron-transfer reaction (d,p). Differential cross sections from (d,p) reactions are compared to reaction calculations to extract the spectroscopic factor (S).

The spectroscopic factor, S, is a measure of the single-neutron shell model component in the wave function of a particular state. Theoretically, it is the norm of the overlap function between the final neutron state and the initial target state. From an experimental perspective, it can be defined as

$$S = (\frac{d\sigma}{d\Omega})_{Exp} \ / \ (\frac{d\sigma}{d\Omega})_{Theory} \tag{1}$$

where $(\frac{d\sigma}{d\Omega})_{Theory}$ is the theoretical prediction for the cross section assuming a specific single-particle configuration for the final neutron state [7]. If experimental and theoretical cross sections agree, then the state is indeed purely single-particle, otherwise the ratio of experiment to theory provides a measure of the fragmentation of single-particle strength. The extraction of S from the data can be strongly model dependent due to the uncertainties in the final neutron state wavefunction. The shape of the effective bound-state potential $V(r)$ is often described as a Woods-Saxon shape, dependent on three parameters: the well depth, V_0 (set to reproduce the neutron binding energy), a radius parameter r_0 which is related to the average radius R through $R = r_0 A^{1/3}$ (A is the mass number of the target) and a, the diffuseness of the potential surface. Standard values for the radius and diffuseness, r_0=1.25 fm and a=0.65 fm, have been used in previous studies (*e.g.* [5, 8–10]). Theoretical cross sections are sensitive to the parameters r_0 and a that define the shape of the bound-state potential. These parameters cannot be constrained by a single (d,p) measurement at peripheral reaction energies.

While the spectroscopic factor is a volume integral of the neutron many-body overlap function, predominantly located in the interior of the nucleus, most (d,p) reactions (in particular those performed with $<\approx$ 12 MeV equivalent energy deuteron beams) are peripheral reactions, that are only sensitive to the tail of this overlap function. This tail can be modeled by a Hankel function with asymptotic normalization coefficient (ANC), $C_{\ell j}$, for a given final state with orbital angular momentum ℓ and total angular momentum j. Since the details of the many-body overlap functions are not generally known, the theoretical calculations are performed for a pure single-particle wavefunction (*i.e.* S = 1). The tail of the single-particle wavefunction is also modeled as a Hankel function, but now with its own single-particle asymptotic normalization coefficient (spANC), $b_{\ell j}$. Changes in the shape of the bound-state potential (*e.g.* r_0, a) affect the single-particle wave functions, producing different values for the spANC, $b_{\ell j}(r_0, a)$. The spANC and the overlap ANC are related to the spectroscopic factor by Eq. 2.

$$C^2_{\ell j} \ = \ S_{\ell j} b^2_{\ell j} \tag{2}$$

Previous studies, for example the (d,p) reaction with 4.5 MeV/u ^{82}Ge and ^{84}Se beams [8], have demonstrated how the spectroscopic factors can change by a factor of 3 or more as a function of realistic values for the spANC, $b_{\ell j}$, while the ANC, $C_{\ell j}$, with this low-energy beam is essentially independent of the Woods-Saxon geometry used to generate the single-particle wavefunction. Given the importance of deducing spectroscopic factors for both nuclear structure and nucleosynthesis, it is crucial to constrain the spANC values (associated with r_0 and a values), which constitutes a dominant uncertainty in the reaction analysis.

A. Combined Method

Mukhamedzhanov and Nunes [11] have proposed measuring the same reaction at two different energies, one (at ∼5 MeV/u) that is peripheral and only probes the asymptotic region of the nucleus, and the other at significantly higher energy (∼40 MeV/u), and therefore, may probe deeper into the nucleus. With the lower energy reaction, the asymptotic normalization coefficient for the nucleus ($C_{\ell j}$) can be directly extracted, with little to no dependence on the geometry of the bound-state potential. However, the spectroscopic factor will have a strong dependence on the choice of bound-state parameters. At higher energy, there is a larger contribution from the interior of the nucleus, but the spectroscopic factor can still be dependent on the shape of the potential, albeit to a lesser degree. The combination of the two measurements allows one to first fix the external portion of the reaction by extracting the $C_{\ell j}$ for a given final state. When the lower energy measurement is combined with that at higher energy, the combined method provides a constraint on the single-particle ANC, $b_{\ell j}$, and the deduced spectroscopic factor, since S is a property of the state in the nucleus and should not be dependent on the energy of the probe. The goal is for the uncertainties in the extracted spectroscopic factor to be dominated by experimental statistics, rather than uncertainties in the effective bound-state potential.

One of the first demonstrations of this combined method was an analysis using previously published data performed by Mukhamedzhanov, Nunes, and Mohr [12],

who compared ^{48}Ca(d,p) cross sections at various energies with neutron capture, ^{48}Ca(n,γ), cross sections. The authors were able to show the sensitivity of S and $C_{\ell j}$ to the single-particle ANC, $b_{\ell j}$, at low and high energies. The combined analysis using the ADiabatic Wave Approximation (ADWA) formalism at both energies indicates a constrained region for the spANC for both the ground- and first-excited states populated in the ^{48}Ca(d,p) ^{49}Ca reaction. From this result, the authors suggested that measurements at ∼30 MeV/u have an interior contribution similar to (n,γ), and both the ANC and spectroscopic factor are important in calculating (n,γ) cross sections. Pang, Nunes, and Mukhamedzhanov [13] pointed out the inconsistencies between the extracted ANC and spectroscopic factor arising from the choice of bound state parameters r_0 and a through both Distorted Wave Born Approximation (DWBA) and ADWA. Reference [13] also found it necessary to first fix the ANC with a peripheral measurement, then extract the spectroscopic factor using non-peripheral reactions. A subsequent test of the combined method by McClesky *et al.* [14] involved the ^{14}C(d,p) reaction in inverse kinematics to deduce properties of the weakly bound ^{15}C. This work indicated that the combined method does yield a constrained region of single-particle ANC for the first excited state of ^{15}C using ADWA. However, this constraint resulted in an unphysical spectroscopic factor (>1.0), which may be attributed to the lack of single-nucleon optical potentials for light nuclei such as ^{14}C. Following the combined method study on states in ^{15}C, Pang and Mukhamedzhanov [15] tested the combined method for deuteron stripping reactions in three different mass regions and also using three different theoretical approaches: DWBA, ADWA, and Continuum Discritized Coupled Channels (CDCC). The authors revealed inconsistencies between the ANC and spectroscopic factor, namely the spectroscopic factors from the combined method were much lower in comparison to previous results. Consequently, the question remains open as to whether the combined method works generally and can provide consistent spectroscopic factors and ANCs, especially for the heavier nuclei important for the r-process. Additionally, it is important to provide further tests of the method on nuclei for which global optical models are better constrained (e.g. A>24 [16–18]).

In the present study, the (d,p) neutron-transfer reaction on ^{86}Kr is used to verify this combined method of extracting spectroscopic information in a mass region well suited for global optical models. ^{86}Kr has a closed N=50 neutron shell; therefore, the low-lying excitations in ^{87}Kr are expected to be single-neutron excitations. Also, global optical parameters have been well characterized in this mass region. The low-energy analysis is based on published studies of the ^{86}Kr(d,p) reaction in normal kinematics at 5.5 MeV/u by Haravu *et al.* [19]. This analysis was combined with a measurement of the (d,p) reaction with a 33 MeV/u ^{86}Kr beam at the National Superconducting Cyclotron Laboratory (NSCL) using the Oak Ridge Rutgers University Barrel Array (ORRUBA) coupled to the S800 magnetic spectrograph.

II. ^{2}H(^{86}Kr,p)^{87}Kr at 33 MeV/u

The ^{2}H(^{86}Kr,p) ^{87}Kr reaction at 33 MeV/u was measured using inverse kinematics at the NSCL. An array of position-sensitive silicon strip detectors was coupled to the S800 magnetic spectrograph to measure charged particles in coincidence with heavy recoils. SIDAR (SIlicon Detector Array) [20] and ORRUBA (Oak Ridge Rutgers University Barrel Array) [21], covered an angular range between 60° and 165° in the laboratory frame as shown by the ungated charged particle spectrum in Fig. 1. Elastically scattered products were detected at angles forward of 90° and were used for beam normalization. The reaction was performed in inverse kinematics, with the ^{86}Kr beam impinging on a thin (∼0.8 mg/cm^2) C_2D_4 foil. The deuterated polyethylene targets were made according to the methods in Ref. [22]. The ejectile protons were detected at backward angles (>90°) in the laboratory. Protons were detected in coincidence with heavy recoils in the S800.

The stable ^{86}Kr beam delivered from the cyclotron was degraded in energy to 33 MeV/u with an average beam rate of 10^6 pps. The total beam rate was limited by the S800 detector system. The upstream and downstream ORRUBA barrels covered angles from 110° - 140° and 65° - 110°, respectively. The ORRUBA detectors are resistive-strip detectors with a position resolution of ∼1 mm, which in the current configuration is approximately ∼ 1° in the laboratory. SIDAR in a lamp-shade configuration consisted of 6 wedge-shaped annular detectors which covered angles between 150° - 170°. Each SIDAR detector has 16 strips with 5-mm pitch; in this configuration, each strip covered roughly ∼1.5° in the laboratory frame.

The detectors were calibrated using alpha particles from a ^{232}U source. The alpha particles from the calibration source were sufficiently energetic that ^{232}U daughter products exited the sealed source into the main scattering chamber. The resulting alpha decays were present during the experiment, as shown by the horizontal lines in Fig. 1. The data shown in Fig. 1 are only charged particle singles events detected in the silicon array, which is meant to show the angular coverage and particle energies; background events come from fusion evaporation of the beam and C_2D_4 target.

A challenge in the present measurement came from complications in merging two separate data acquisition systems during the experiment, namely the NSCLDAQ for the S800 and the silicon detectors that used the NSCL version of the ASICs (Application Specific Integrated Circuits) system that was developed to handle a large number of readout channels by collaborators at Washington University - St. Louis [23, 24]. As mentioned above, the alpha decays from the daughter products of

the ^{232}U calibration source were visible throughout the experiment, which unfortunately overlapped the region where the ejectile protons from the (d,p) reaction would be observed at the most backward angles. The random alpha events should have been significantly suppressed by requiring coincidence events between the ejectile proton and the heavy recoil in the S800; however, due to the complications in merging the two data acquisition systems, the coincidence settings were shifted during the experiment which resulted in a significant loss of coincident events.

Figure 2 shows a Q-value spectrum from a small subset of the data where reliable coincidence events between ORRUBA and the S800 were recorded. Charged particle singles events were recorded during the entire experiment, and differential cross sections were extracted for proton energies and angles where the alpha energies did not interfere and the fusion evaporation background was sufficiently flat.

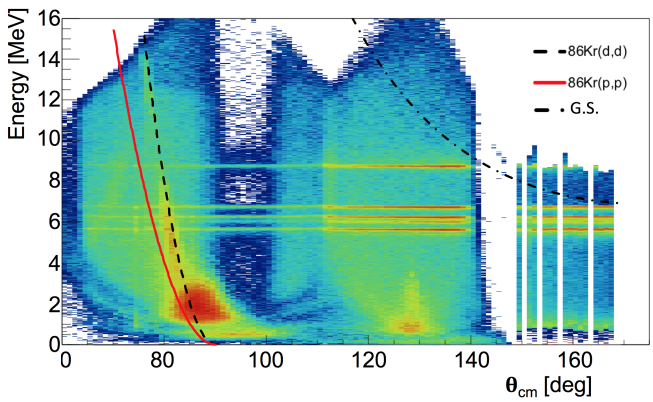

FIG. 1. (color online) Particle energy as a function of laboratory angle for singles events in the silicon detector arrays. Overlayed lines are kinematics calculations for elastic scattering and for the population of the ground state in ^{87}Kr. The gap in data at 90° is shadow from the target ladder. Horizontal lines are from the daughter products from the ^{232}U calibration sealed source that contaminated the inner walls of the scattering chamber

The Q-value spectrum in Fig. 2 is fit for the states of ^{87}Kr at the energies adopted from Ref. [19]. The excitation energies of states in ^{87}Kr measured in this work were consistent with those of previous measurements. The center of mass energy resolution is $\Delta E_{c.m.} \approx 400$ keV FWHM; therefore, the ground- and first-excited states (E_x=0.53 MeV) are not well resolved. The energy resolution shown in Fig. 2 suffers from the intrinsic resolution of the detectors, as well as the thickness of the target used (*e.g.* ~0.8 mg/cm^2). The target thickness was chosen to mimic the conditions expected when using radioactive ion beams, with low beam intensities (~10^4-10^5 pps) and low cross sections (<≈ mb).

The bulk of the data available for analysis was the charged-particle singles events, with no S800 heavy recoil gating that would have served to reduce background

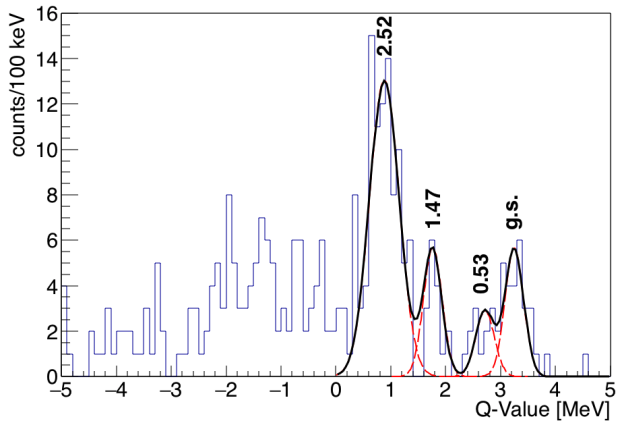

FIG. 2. Q-value spectrum from a subset of the data. Ground state Q-value is 3.29 MeV. Excited state energies are labeled above the fitted peak. Background is mitigated by excluding the alpha contamination events as well as gating on coincidence events in the S800 magnetic spectrograph.

from fusion evaporation and the contaminant alphas. The background was sufficiently flat at laboratory angles greater than 145 degrees and the background to peak ratio for the ground state was less than 0.5. Background events increased exponentially toward 90 degrees but the ground state peak was still apparent with a background to peak ratio of 0.6. A state at 2.5 MeV in excitation energy was also visible above background for laboratory angles between 110 and 140 degrees with a background to peak ratio of less than 0.5. Therefore, the analysis was focused on the ground-state and 2.5 MeV excited state assumed to be the $7/2^+$ state observed in previous work [19, 25].

Angular distributions were extracted for the ground- and 2.5 MeV excited states (Fig. 3). Charged-particle counts for each excited state were summed in a given angular range. The (d,d) elastic scattering rate was used to ascertain the incident beam rate and normalize charged particle counts for a given angular bin. Using a timing scintillator, the particle rate of the incoming beam was calibrated to the current reading of a Faraday cup that could operate at the high incoming particle rate during production runs. Charge states of the degraded ^{86}Kr beam are separated in the A1900 fragment separator. The Faraday cup was positioned to intercept the 36^+ charge state of the beam, while the 35^+ charge state was sent to the experiment. The extracted cross section was normalized using the (d,d) elastic scattering rate calibrated to the rate on the Faraday cup, and did not rely on the scattering cross section being Rutherford. The uncertainties in the cross sections shown in Fig. 3 are statistical.

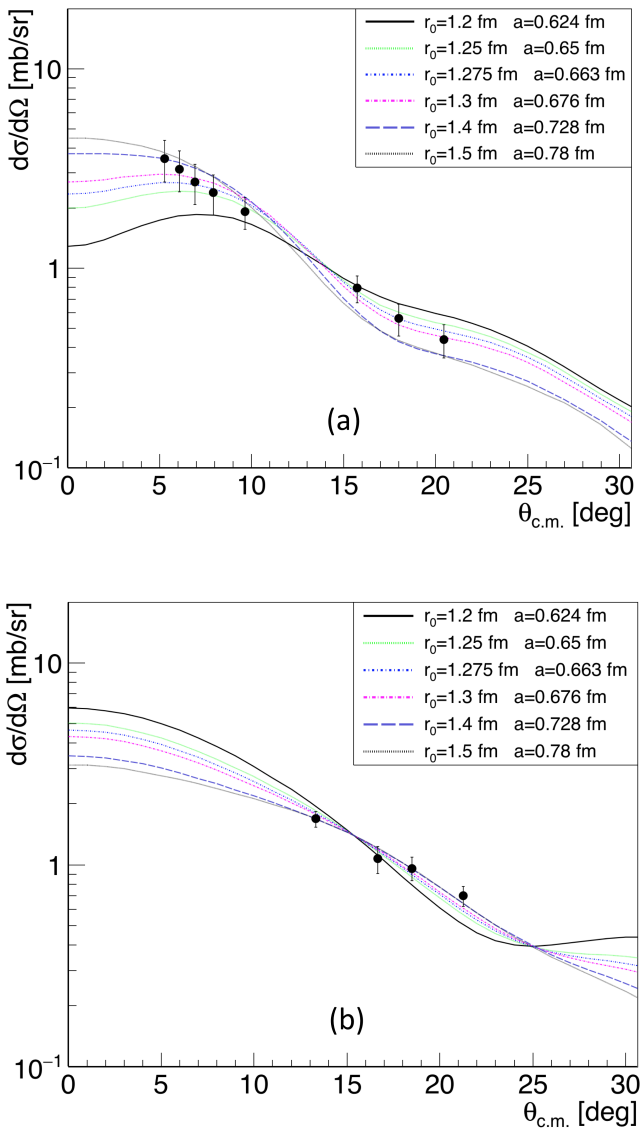

FIG. 3. Differential cross sections as a function of center of mass angle for the (d,p) reaction with 33 MeV/u ^{86}Kr beams and compared to FR-ADWA calculations (lines) described in section III. The theoretical cross sections for each (r_0,a) pair were scaled using a least squares fit to the data points to deduce S for each state. (a) $5/2^+$ ground state of ^{87}Kr (points). FR-ADWA calculations assume ℓ=2, $2d_{5/2}$ transfer and varied radius and diffuseness parameters for the neutron bound state. (b) $7/2^+$ 2.5 MeV state of ^{87}Kr (points). FR-ADWA calculations assumed ℓ=4, $1g_{7/2}$ transfer and varied radius and diffuseness parameters for the neutron bound state.

III. ANALYSIS DETAILS

The Finite-Range ADiabatic Wave Approximation (FR-ADWA) [26] was used to analyze the ^{86}Kr(d,p) reactions at both energies. This approach takes into account the breakup of the deuteron and has been shown to perform well for deuteron energies >10 MeV [27]. Modern global optical parameterizations of Koning-Delaroche (KD) [18] were used for the nucleon-target potential at both the low and high energy, together with the Reid soft-core potential [28] for the nucleon-nucleon interaction. Optical model parameters used in this work are summarized in Table I. As shown in Table II, the neutron bound state parameters were varied over the range r_0= 1.2 - 1.5 fm and a= 0.624 - 0.78 fm to span single-particle ANCs ($b_{\ell j}$) for three final states of ^{87}Kr from the (d,p) reaction. The geometry of the real central interaction was also used for the bound state spin-orbit geometry. TWOFNR [29] was used to generate the theoretical cross sections, which only introduces a finite-range correction. FRESCO [30] was used to verify the calculated cross sections, which incorporates a full treatment of the finite-range transfer and was found to produce the same cross sections as TWOFNR in the angular range of interest; therefore the analysis was performed using only TWOFNR. The same range of bound-state configurations, and therefore same spANC values, were used in the analysis of both the low- and high-energy measurements of the ^{86}Kr$(d,p)^{87}$Kr reaction.

Theoretical cross sections with varying (r_0,a) pairs from this FR-ADWA framework are displayed in Fig. 3. The calculated cross sections were normalized to the data using a least squares method. An ℓ=2, $2d_{5/2}$ transfer and a J^π=$5/2^+$ assignment for the ground state of ^{87}Kr were adopted from Refs. [19, 25]. Additionally, an ℓ=4, 1g7/2 transfer and a J^π=$7/2^+$ assignment was adopted from Ref. [19] for the excited state at E_x=2.52 MeV.

A. Extracting the ANC: ^{86}Kr$(d,p)^{87}$Kr at 5.5 MeV/u

Angular distributions reported by Haravu *et al.* [19] were used to extract the nuclear ANC $C_{\ell j}$ and constrain the asymptotic behavior of the wavefunctions. The $2d_{5/2}$ ground-state and $1g_{7/2}$ excited-state differential cross sections are shown in Figs. 4a and 4b, respectively. Each angular distribution is overlayed with FR-ADWA calculated cross sections for the different bound state configurations in Table II. To be consistent with the high energy analysis, each FR-ADWA calculated cross section was normalized to the data by a least squares minimization for center of mass (c.m.) angles <90°. The angular cutoff was chosen to constrain the region where ADWA is more robust (i.e. low center of mass angles, excluding higher order effects) and to provide a more stringent constraint to the data rather than normalizing to the data in the first peak only.

B. Determination of S from combined measurements

To constrain the single-particle ANC and deduce spectroscopic factors with uncertainties dominated by exper-

TABLE I. Koning-Delaroche global optical model parameters [18] used for the exit channel and to construct the adiabatic potentials for the deuteron using the adiabatic treatment of Johnson-Tandy [26]

	V [MeV]	r_0 [fm]	a_0 [fm]	W [MeV]	r_W [fm]	a_W [fm]	W_s [MeV]	r_{ws} [fm]	a_{ws} [fm]	V_{so} [MeV]	r_{so} [fm]	a_{so} [fm]	W_{so} [MeV]	r_{soi} [fm]	a_{soi} [fm]
n	39.467	1.212	0.665	2.924	1.212	0.665	4.987	1.272	0.530	5.224	1.039	0.590	-0.200	1.039	0.590
p	48.423	1.212	0.665	3.103	1.212	0.665	7.156	1.272	0.563	5.262	1.039	0.590	-0.184	1.039	0.590
^{87}Kr+p (g.s)	36.055	1.212	0.665	7.288	1.212	0.665	3.514	1.272	0.564	4.566	1.039	0.590	-0.568	1.039	0.590

TABLE II. Values of single-particle ANC, $b_{\ell j}$, for each choice of radius and diffuseness parameters for the ground $5/2^+$, first-excited $1/2^+$ and 2.52-MeV $7/2^+$ states in ^{87}Kr.

r_0 [fm]	a [fm]	$b_{d5/2}$ [fm$^{-1/2}$]	$b_{s1/2}$ [fm$^{-1/2}$]	$b_{g7/2}$ [fm$^{-1/2}$]
1.2	0.624	5.35	11.06	0.134
1.225	0.637	5.70	11.62	0.146
1.25	0.65	6.08	11.90	0.158
1.275	0.663	6.45	12.83	0.172
1.3	0.676	6.90	13.48	0.185
1.325	0.689	7.35	14.16	0.200
1.35	0.702	7.82	14.87	0.216
1.375	0.715	8.32	15.62	0.233
1.4	0.728	8.85	16.41	0.251
1.45	0.754	10.0	18.10	0.290
1.5	0.78	11.27	19.96	0.334

TABLE III. Summary of spectroscopic properties of excitations in ^{87}Kr from the present analysis and the measurements by Haravu and collaborators at 5.5 MeV/u [19]. The excitation energies and J^π assignments are adopted values [31]. Spectroscopic factors, S, from Ref. [19] as well as nuclear ANCs ${C_{\ell j}}^2$ from this work, are tabulated. Ref. [19] did not quote uncertainties on S values.

E_x [MeV]	J^π	S (Ref.[19])	${C_{\ell j}}^2$ [fm^{-1}]
0.0	$5/2^+$	0.56	18(2)
0.53	$1/2^+$	0.46	89(10)
2.52	$7/2^+$	0.49	0.0120(10)

imental uncertainties, the following procedure was used. First, a spectroscopic factor was obtained through Eq. 1 by normalizing the FR-ADWA prediction to the experimental cross section for each set of (r_0,a) (or spANC $b_{\ell j}$) values summarized in Table II. The corresponding many-body ANC ($C_{\ell j}$) was deduced from the relation in Eq. 2. The results from the FR-ADWA analysis of both the low- and high-energy measurements for the extracted spectroscopic factors and nuclear ANCs for the ground state of ^{87}Kr are shown in Fig. 5.

For the low-energy results, the spectroscopic factor varies by about a factor of four as the bound-state potential geometry changes with increasing spANC. The ANC is relatively constant over the range of $b_{\ell j}$, consistent with the expectation that the reaction is peripheral at 5.5 MeV/u. Table III summarizes the extracted $C^2_{\ell j}$ values from the present FR-ADWA analysis for the ground- ($2d_{5/2}$), first-excited ($3s_{1/2}$) and 2.5 MeV ($1g_{7/2}$) states measured at 5.5 MeV/u in Ref. [19]. Uncertainties come from the least squares fit to the data (∼1 %), a total systematic error adopted from Ref. [19] (6%), and an assumed uncertainty for the FR-ADWA calculation (10%). The spectroscopic factors reported in Ref. [19] were deduced from optical-model parameters based on a fit to elastic scattering and a traditional DWBA approach, which does not account for deuteron breakup.

In contrast to the lower energy analysis, the ANC is not constant over the range of $b_{\ell j}$ for the higher energy results. Since $C_{\ell j}$ and S are properties of a nuclear state, independent of the reaction by which they are determined, the correct bound-state potential geometry should yield consistent $C_{\ell j}$ and S values from measurements at different energies. Therefore, the crossing in Fig. 5 constrains the single-particle ANC to $b_{d5/2}$=6.46 $^{+1.12}_{-0.57}$ fm$^{-1/2}$. The Chapel-Hill parameterization (CH89) was also used to confirm this constrained single-particle ANC, and the constrained spANC from each optical model parameterization is shown in Table IV.

TABLE IV. Constrained single-particle ANC values for the ^{87}Kr $5/2^+$ ground state calculated with KD [18] and CH89 [17] optical model potentials

Global optical model	$b_{d5/2}$ [fm$^{-1/2}$]
Koning-Delaroche [18]	6.46 $^{+1.12}_{-0.57}$
Chapel-Hill [17]	6.70 $^{+1.30}_{-0.63}$

The constrained value for the single-particle ANC for the ground state does not correspond to a unique set of radius and diffuseness parameters, rather many different combinations will produce the same spANC. In order to show that the spANC, and hence the bound-state potential, are constrained with this combined method, a very large set of radius and diffuseness parameters was used to span the entire physical range of bound-state geometries. The same procedure described in Section III was followed to extract the spectroscopic factor and many-body ANC for every bound-state configuration. The results are shown by the surfaces in Fig. 6, where the extracted spectroscopic factors and many-body ANCs are shown as a function of radius and diffuseness parameters.

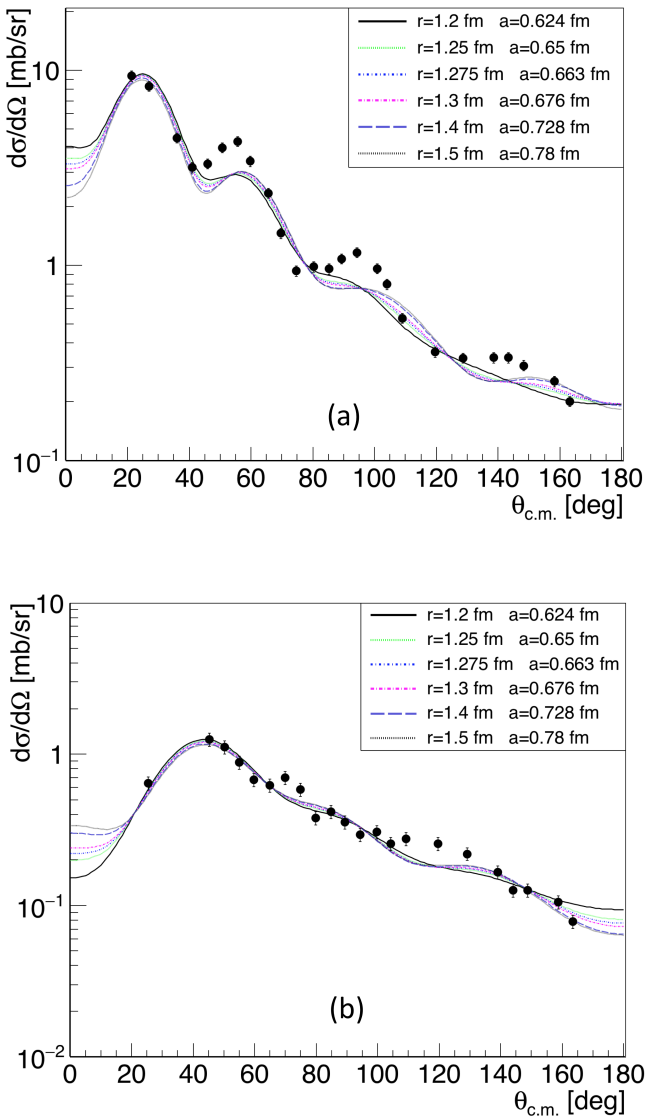

FIG. 4. Differential cross sections from the 5.5 MeV/u ^{86}Kr(d,p) reaction measurement in Ref. [19] as a function of center of mass angle and compared to FR-ADWA calculations (lines). (a) $5/2^+$ ground state of ^{87}Kr (points). FR-ADWA calculations assume ℓ=2, $2d_{5/2}$ transfer. (b) $7/2^+$ excited state of ^{87}Kr (points). FR-ADWA calculations assume ℓ=4, $1g_{7/2}$ transfer. Each of the calculated cross sections varied parameters (r_0,a) for the neutron bound state. The theoretical cross section were scaled using a least squares fit to the data points for c.m. angles <90° to deduce S for each (r_0,a) pair.

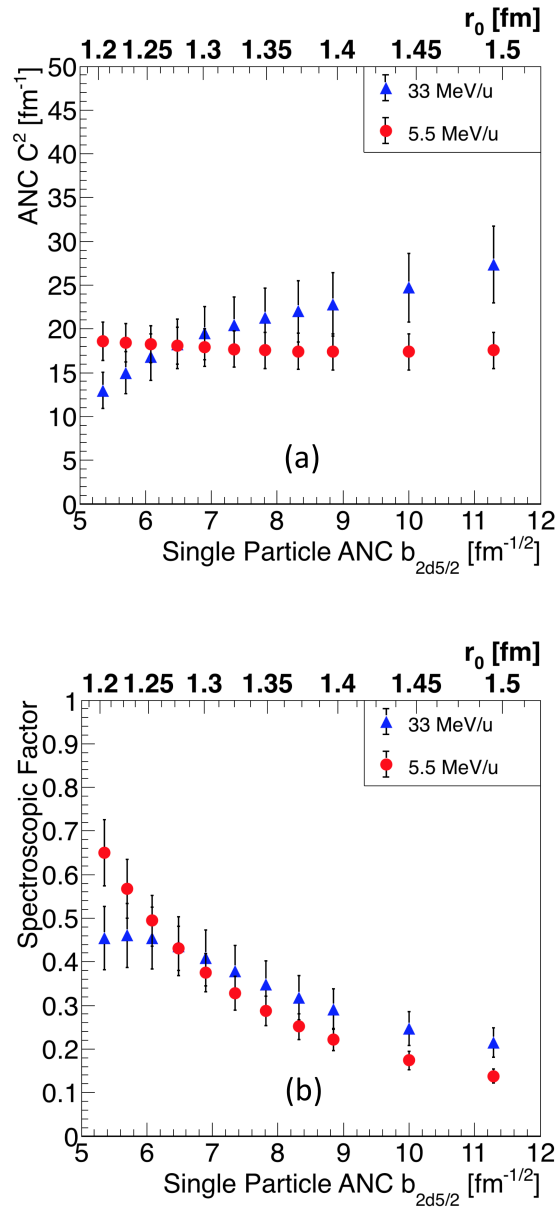

FIG. 5. (Color online). Results from the FR-ADWA analysis with KD optical model parameters for the ^{87}Kr ground-state from measurements at 5.5 MeV/u (red) and 33 MeV/u (blue). (a) Nuclear ANC $C^2_{\ell j}$ values as a function of single-particle ANC $b_{\ell j}$. (b) Spectroscopic factors as a function of single-particle ANC $b_{\ell j}$.

The original chosen set of parameters from Table II are also shown by the points in Fig. 6.

The crossing of these surfaces, shown by the solid line in Fig. 6, describes a range of values for r_0 and a that will produce the experimentally constrained value for the single-particle ANC. The same parameters for the surfaces in Fig. 6 are displayed in Fig. 7 in order to clearly distinguish the values of the spANC in the surface crossing region. Overlayed in Fig. 7 are lines of constant diffuseness to show the region of (r_0, a) that produce the constrained spANC. The uncertainty bands in the surface crossing region are produced by shifting the high energy surface ±10%, based on an assumed uncertainty for the FR-ADWA calculation.

The surface crossing region in Fig. 7 shows that for a relatively large range of physical (r_0, a) values, the

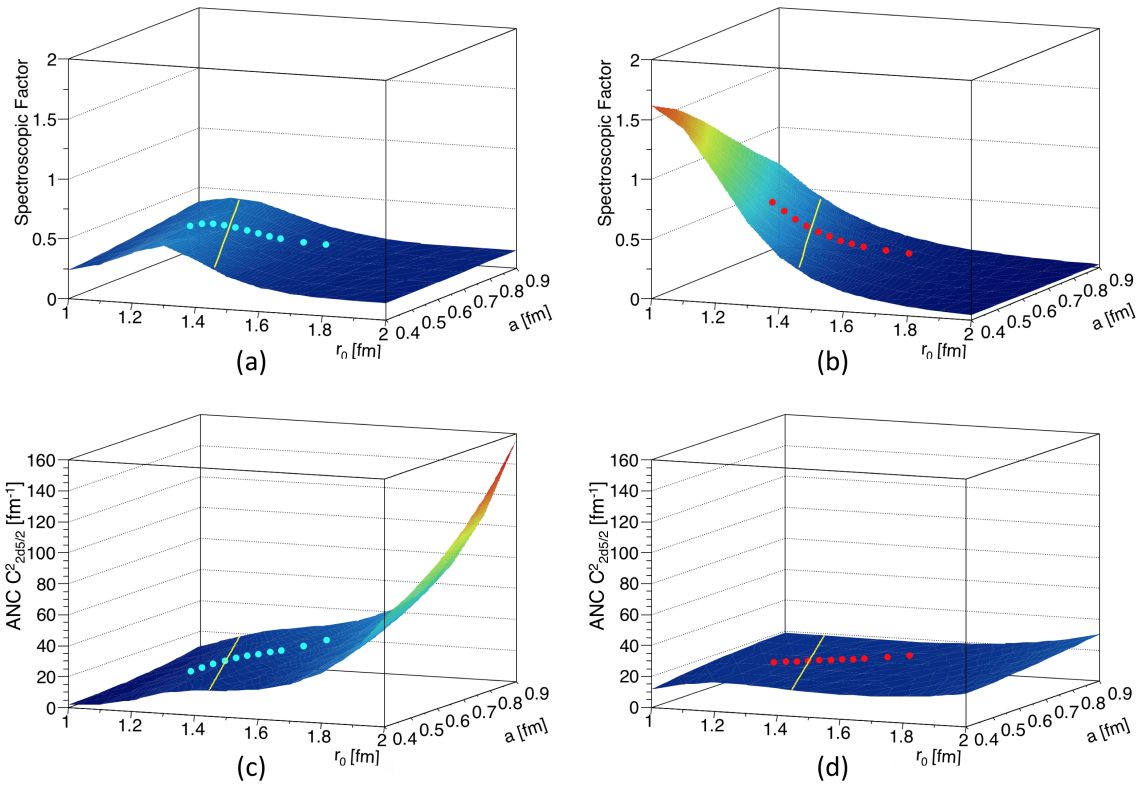

FIG. 6. (Color online) Contour plots of the ^{87}Kr ground-state spectroscopic factor and many-body ANC as functions of r_0 and a. Points in each panel represent the initial set of parameters described in Table II. Surfaces show the entire spanned region for every (r_0, a) pair. Panels (a) and (b) show the extracted spectroscopic factors for the high and low energy measurements, respectively. Panels (c) and (d) show the many-body ANC for the high and low energy measurements, respectively. The line marks the crossing region of the high and low beam energy surfaces.

single-particle ANC remains constant. Different types of scattering experiments would be needed to constrain the values for the radius and diffuseness, which should be consistent with the combined method deduced single-particle ANC for the ground state of ^{87}Kr.

A constrained value for the radius and diffuseness can be extracted based solely on the original set of parameters in Table II, and is displayed by the single point in Fig. 8. Using the Table 8 parameters, the constrained bound-state parameters are $r_0 = 1.27^{+0.07}_{-0.04}$ fm and $a = 0.66^{+0.04}_{-0.02}$ fm where the uncertainties are based on the uncertainties in the constrained value for the ^{87}Kr ground state spANC. It is noteworthy that these parameter values are in good agreement with the canonical values of r_0= 1.25 fm and a= 0.65 fm. Also displayed in Fig. 8 is the surface crossing region and uncertainty bands from Fig. 6, to show the exact range of r_0 and a values that can reproduce the same value for the constrained spANC. Colored contour bands in Fig. 8 show the approximate value for the spANC at each value of radius and diffuseness; note that we have constrained $b_{d5/2}$=6.46 $^{+1.12}_{-0.57}$ fm$^{-1/2}$.

Adopting the constrained single-particle ANC value for the bound-state configuration of the ground-state reaction yields a spectroscopic factor of S=0.44 $^{+0.09}_{-0.13}$, where the uncertainty comes from the least squares fit to the data (∼7 %), a total systematic uncertainty of 10% (*e.g.* target thickness, beam normalization) and an assumed uncertainty for the FR-ADWA calculation (10%).

C. Combined results for the 2.5 MeV excited state

Figure 9 summarizes the results for the dependences of both $C_{\ell j}$ and S as a function of $b_{\ell j}$ for the excited state at E=2.5 MeV, where a $1g_{7/2}$ ℓ=4 transfer is assumed based on previous studies.

In contrast to the results for the ground-state ℓ=2 transfer, both the low and higher energy measurements yield statistically identical results, including a relatively flat $C_{\ell j}$ which is a signature of a peripheral reaction even at 33 MeV/u. The apparent peripheral nature of the ℓ=4 transfer in the NSCL data could be attributed to the larger angular momentum transfer, indicating that the centrifugal barrier has a significant effect, even at these higher energies. Also, the measured differential cross section covers only a small angular range, where the shapes of the FR-ADWA predictions for different (r_0,a) pairs are

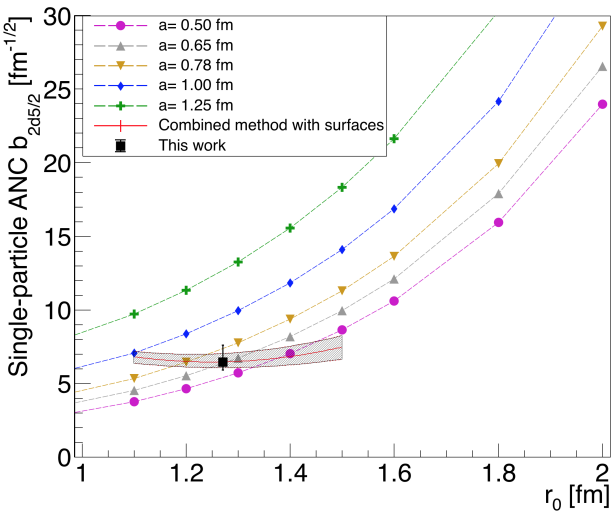

FIG. 7. (Color online) Single-particle ANC for the ^{87}Kr ground state as a function of radius parameter, r_0 overlayed with lines of constant diffuseness, a. The original constrained value from the (r_0, a) parameter set from Table II is shown by the black box. The crossing region from the surfaces in Fig. 6 is shown by the red line. Uncertainty bands are described in the text.

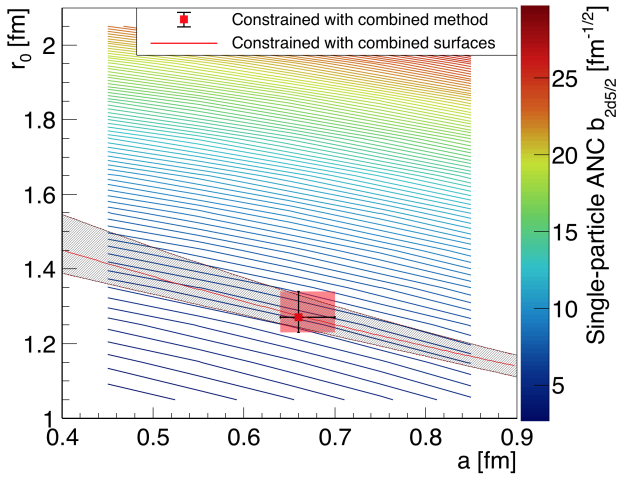

FIG. 8. (Color online) Contour bands of the ^{87}Kr ground state single-particle ANC corresponding to the radius parameter, r_0, as a function of diffuseness, a. The red data point with the black uncertainty bars corresponds to the $r_0 = 1.27^{+0.07}_{-0.04}$ fm and $a = 0.66^{+0.04}_{-0.02}$ fm value deduced from the analysis with the radius and diffuseness values in Table II. The shaded band with red line central values represents the range of (r_0,a) values that correspond to the constrained spANC value $b_{d5/2}$=6.46 $^{+1.12}_{-0.57}$ fm$^{-1/2}$.

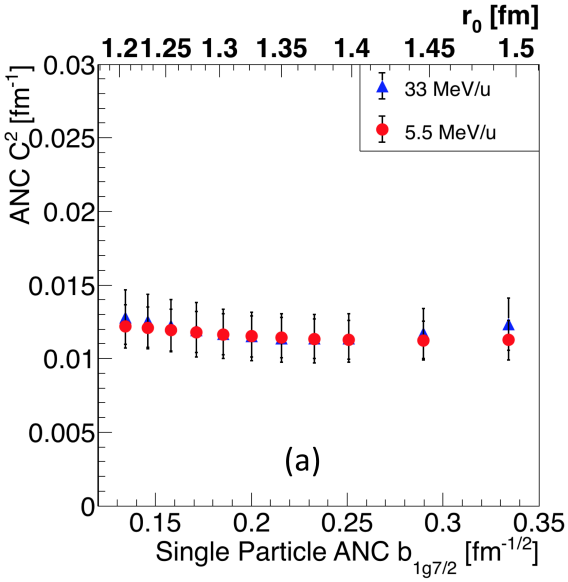

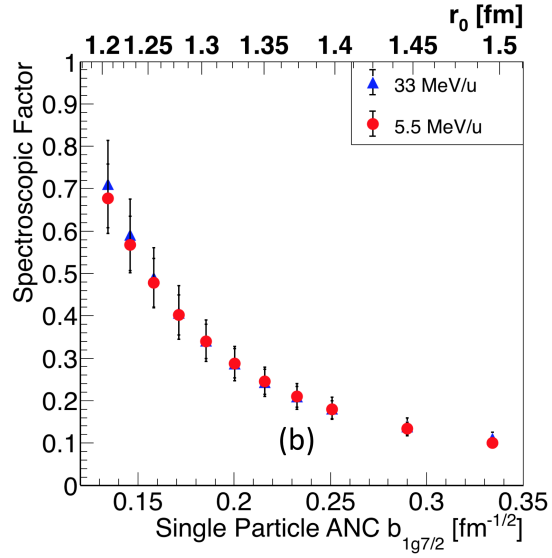

FIG. 9. (Color online). Results from the FR-ADWA analysis of the ^{87}Kr 2.5 MeV $1g_{7/2}$ state measurements at 5.5 MeV/u (red) and 33 MeV/u (blue). (a) Nuclear ANC ${C_{\ell j}}^2$ values as a function of single-particle ANC $b_{\ell j}$. (b) Spectroscopic factors as a function of single-particle ANC $b_{\ell j}$.

relatively similar (see Fig. 3b). Data at smaller (<10°) and/or larger (>25°) c.m. angles, where the shapes of the FR-ADWA predictions are more distinctive for different (r_0,a) values, may have provided more significant differences in S as a function of (r_0,a) in the higher energy data and therefore a constraint on the bound-state potential parameters.

In Table V, the extracted spectroscopic factors for the $5/2^+$ ground and $7/2^+$ excited states in ^{87}Kr are compared to previous measurements at lower beam energy. Since there was no constrained value for the spANC for the 2.5 MeV state, the spectroscopic factor shown in Table V was calculated assuming the r_0 and a values deduced for the ground state from the analysis with the Table II values. The effective mean field is not necessarily the same for the different states if there are strong

correlations; ideally a constrained region for the spANC is desired for every excited state. The spectroscopic factors deduced in the present work are within uncertainties similar to, although consistently lower, than previous results. The similarity may be due to the similarity between the (r_0, a) values used in the traditional DWBA analysis to the (r_0, a) values constrained in the present work with the Table II analysis. That the spectroscopic factors are lower has been previously observed for the combined method analysis in [15].

TABLE V. Summary of spectroscopic factors for the $5/2^+$ ground and excited $7/2^+$ states of ^{87}Kr from the present analysis and previous measurements at lower beam energies.

Reference	Energy [MeV/u]	$S_{d5/2}$ (g.s.)	$S_{g7/2}$ (E_x=2.5 MeV)
[19]	5.5	0.56	0.49
[25]	7.5	0.66	-
[32]	10	0.63±0.16[a]	0.58±0.15[b]
This work	33	$0.44\ ^{+0.09}_{-0.13}$	$0.41\ ^{+0.08}_{-0.12}$

[a] Adopted from the normalization factor for J^π=$5/2^+$
[b] Adopted from the normalization factor for ℓ=4 transitions

IV. SUMMARY

The ^{86}Kr$(d,p)^{87}$Kr reaction was measured in inverse kinematics at 33 MeV/u at the National Superconducting Cyclotron Laboratory with the ORRUBA detector system coupled to the S800 spectrograph. The results from this measurement were combined with those from an earlier study at 5.5 MeV/u [19] to test the combined method proposed by Mukhamedzhanov and Nunes [11] to extract spectroscopic factors by providing a constraint on the parameters of the neutron bound-state potential. The present work demonstrates that for lower angular momentum, at least ℓ=2 transfer, the spANC, and hence the bound-state potential, can be constrained from ^{86}Kr(d,p) measurements at two energies using the combined method. A single-particle ANC of $b_{d5/2}$=$6.46\ ^{+1.12}_{-0.57}$ fm$^{-1/2}$ was constrained for the ground state of ^{87}Kr, and therefore the spectroscopic factor S=$0.44\ ^{+0.09}_{-0.13}$ was deduced. The spectroscopic factor extracted in this work for the $5/2^+$ ground state from the present combined method analysis is somewhat lower than previous analyses, which made assumptions on the configuration of the bound-state potential. For the ℓ=4 transfer to the 2.5 MeV state, it appears that the reaction, even at 33 MeV/u, remains peripheral which could be due to the higher centrifugal barrier to transfer.

Spectroscopic factors determined with a reduced dependence on the bound-state potential for relatively low ℓ transfers will impact calculations of direct neutron capture rates on nuclei with low level densities near the neutron separation energy and near the waiting points during freeze-out from an r-process event. The present work has demonstrated that by combining measurements at two very different beam energies the spANC $b_{\ell j}$ and hence spectroscopic factors can be deduced with greater certainty. Next steps could include determining the spectroscopic factors, and associated direct-semidirect neutron capture cross sections near neutron closed shells, deduced from the combined method in neutron-rich nuclei. The first of such steps could be realized for neutron-rich ^{85}Se where the peripheral ^{84}Se(d,p) reaction has been analyzed [8] and the (d,p) reaction with 45 MeV/u ^{84}Se beams has recently been measured [33].

V. ACKNOWLEDGMENTS

The authors would like to thank Jeromy Tompkins for his outstanding effort and long hours during the experiment.

This work was supported in part by the National Science Foundation NSF-PHY-1404218 (Rutgers), NSF-PHY-1068571 (MSU), NSF-PHY-1403906 (MSU), NSF-PHY-1102511 (NSCL), and NSF-PHY-1419765 (Notre Dame), and the U.S. Department of Energy National Nuclear Security Administration Stewardship Science Academic Alliances under cooperative agreement Nos. DE-NA0002132 and DE-FG52-08NA28552 (Rutgers, MSU) and Office of Nuclear Physics under contracts Nos. DE-AC05-00OR22725 (ORNL), DE-FG02-96ER40983 (UTK), DE-SC0001174 (UTK), and DE-FG02-96ER40955 (TTU).

[1] M. R. Mumpower, R. Surman, G. C. McLaughlin, and A. Aprahamian, Prog. Part. Nucl. Phys. **86**, 86 (2016), [Erratum: Prog. Part. Nucl. Phys. **87**, 116 (2016)].
[2] R. Surman, M. Mumpower, R. Sinclair, K. L. Jones, W. R. Hix, and G. C. McLaughlin, AIP Advances **4**, 041008 (2014).
[3] G. Satchler, *Direct Nuclear Reactions* (Clerendon Press, 1983).
[4] N. Austern, *Direct Nuclear Reaction Theories* (John Wiley and Sons Inc, 1970).
[5] R. L. Kozub *et al.*, Phys. Rev. Lett. **109**, 172501 (2012).
[6] B. Manning *et al.*, Phys. Rev. C. Rapid Communication (2019), in press.
[7] I. J. Thompson and F. M. Nunes, *Nuclear reactions for astrophysics: principles, calculation and applications of low-energy reactions* (Cambridge Univ. Press, Cambridge, 2009).
[8] J. S. Thomas *et al.*, Phys. Rev. C **76**, 044302 (2007).
[9] K. L. Jones *et al.*, Phys. Rev. C **84**, 034601 (2011).
[10] F. Lu *et al.*, Phys. Rev. C **88**, 017604 (2013).

[11] A. M. Mukhamedzhanov and F. M. Nunes, Phys. Rev. C **72**, 017602 (2005).
[12] A. M. Mukhamedzhanov, F. M. Nunes, and P. Mohr, Phys. Rev. C **77**, 051601 (2008).
[13] D. Y. Pang, F. M. Nunes, and A. M. Mukhamedzhanov, Phys. Rev. C **75**, 024601 (2007).
[14] M. McCleskey *et al.*, Phys. Rev. C **89**, 044605 (2014).
[15] D. Y. Pang and A. M. Mukhamedzhanov, Phys. Rev. C **90**, 044611 (2014).
[16] J. Lohr and W. Haeberli, Nuclear Physics A **232**, 381 (1974).
[17] R. Varner, W. Thompson, T. McAbee, E. Ludwig, and T. Clegg, Physics Reports **201**, 57 (1991).
[18] A. Koning and J. Delaroche, Nuclear Physics A **713**, 231 (2003).
[19] K. Haravu, C. L. Hollas, P. J. Riley, and W. R. Coker, Phys. Rev. C **1**, 938 (1970).
[20] D. W. Bardayan *et al.*, Phys. Rev. C **63**, 065802 (2001).
[21] S. D. Pain *et al.*, AIP Conference Proceedings **1090**, 570 (2009).
[22] M. Febbraro, D. Walter, S. Shadrick, S. Pain, K. Chipps, C. Thornsberry, and E. Lesser, Nuclear Instruments and Methods in Physics Research Section B: Beam Interactions with Materials and Atoms **410**, 53 (2017).
[23] G. L. Engel, M. Sadasivam, M. Nethi, J. M. Elson, L. G. Sobotka, and R. J. Charity, Nuclear Instruments and Methods in Physics Research Section A: Accelerators, Spectrometers, Detectors and Associated Equipment **573**, 418 (2007).
[24] M. Wallace, M. Famiano, M. van Goethem, A. Rogers, W. Lynch, J. Clifford, F. Delaunay, J. Lee, S. Labostov, M. Mocko, L. Morris, A. Moroni, B. Nett, D. Oostdyk, R. Krishnasamy, M. Tsang, R. de Souza, S. Hudan, L. Sobotka, R. Charity, J. Elson, and G. Engel, Nuclear Instruments and Methods in Physics Research, Section A: Accelerators, Spectrometers, Detectors and Associated Equipment **583**, 302 (2007).
[25] R. E. Sass, B. Rosner, and E. J. Schneid, Phys. Rev. **138**, B399 (1965).
[26] R. Johnson and P. Tandy, Nuclear Physics A **235**, 56 (1974).
[27] F. M. Nunes and A. Deltuva, Phys. Rev. C **84**, 034607 (2011).
[28] R. V. Reid, Annals of Physics **50**, 411 (1968).
[29] J. Tostevin, "University of surrey version of the code *twofnr* (of m. toyama, m. igarashi and n. kishida) and code front," private communication (2014).
[30] I. J. Thompson, Computer Physics Reports **7**, 167 (1988).
[31] T. Johnson and W. Kulp, Nucl. Data Sheets **129** (2015).
[32] D. K. Sharp *et al.*, Phys. Rev. C **87**, 014312 (2013).
[33] D. Walter *et al.*, NSCL experiment 16025 completed (2017).